ELSEVIER

Fluid Dynamics Research 26 (2000) 157–179

FLUID DYNAMICS RESEARCH

A monopolar vortex encounters a north–south ridge or trough

J.H.G.M. van Geffen *, P.A. Davies

Department of Civil Engineering, University of Dundee, Nethergate, Dundee DD1 4HN, UK

Received 2 March 1998; received in revised form 29 January 1999; accepted 17 March 1999

Abstract

Results are described from a two-dimensional numerical model in which a cyclonic monopole that moves due to the β-effect encounters a north–south oriented ridge or trough, the height and depth of which is varied. The fate of the monopole depends on its initial north–south position y_0 (or, equivalently, the value of the constant f_0 in the Coriolis parameter): the monopole can be rebounded, destroyed or trapped by the topography. Only for a narrow range of y_0-positions, depending on the height (depth) of the ridge (trough), can the monopole actually cross the topography, sometimes after being heavily deformed. It is the gradient of the topography-induced vorticity, which deforms the background potential vorticity field due to the β-effect, that determines the fate of the monopole. This topography-induced vorticity is larger for initial positions more to the north or south, and for higher ridges and deeper troughs.

PACS: 47.32.Cc; 47.11.+j

Keywords: Vortex dynamics; Computational methods in fluid dynamics

1. Introduction

Field observations (see e.g. Richardson 1993a,b; Bower et al., 1995; Kamenkovich et al., 1996; Bograd et al., 1997) have shown the widespread existence of several kinds of oceanic vortices, such as, for example, Meddies, Gulf Stream eddies and anticyclones, and Agulhas eddies. These vortices are relatively abundant; Richardson (1993b) estimates that there are roughly 1000 discrete eddies in the North Atlantic. Many are created in frontal regions and they are thought to play an important role in the horizontal transport of quantities such as heat, momentum, salt and pollutants. The vortices move due to a combination of the latitudinal (y) variation of the Coriolis parameter f (the so-called β-effect) and the general background oceanic flow. As such vortices move, they inevitably interact

* Corresponding author. Present address: Royal Netherlands Meteorological Institute, P.O. Box 201, 3730 AE De Bilt, The Netherlands.
E-mail address: jos@tnj.phys.tue.nl (J.H.G.M. van Geffen)

0169-5983/00/$20.00
PII: S0169-5983(99)00022-2

with submarine topographic features, and these interactions are known to influence the trajectories of the vortices (with the possibility that the vortex may be destroyed by the topographic encounter).

Van Geffen and Davies (1999) — hereafter named VGD — employed a simple one-layer two-dimensional (shallow water) model to study the basic features of vortex–topography interactions. They considered a cyclonic monopolar vortex encountering a smooth ridge with variable height, width and orientation on a pure β-plane (i.e. with Coriolis parameter $f = \beta y$) and showed, for example, that a north–south oriented ridge has a much larger impact on the monopole's evolution than an east–west oriented counterpart, under otherwise-identical conditions. VGD showed that the influence of the north–south ridge depends on the width and height of the ridge and reported that whereas the monopole can cross a low ridge with some disturbance to its trajectory, sufficiently high ridges cause topography-induced flow deformations that can lead to the disintegration of the vortex.

For cases of finite height topography where the monopole crosses the north–south ridge after significant topographic interaction, VGD concluded that such behaviour is determined crucially by whether the vortex has gathered sufficient positive potential vorticity on its (north)west side by moving north along the ascending (east) side of the ridge. A question that then naturally arises is whether the *initial* position of the monopole in the north–south direction (the y-coordinate) influences the monopole's evolution. The study described in the present paper investigates this point, for cases in which the width and orientation of the ridge are kept fixed but the height is varied; cases of negative heights (i.e. troughs) are included in this study. The other point left open by VGD is the influence of a non-zero f_0 on the evolution of the monopole, where f_0 is the constant part of the Coriolis parameter: $f = f_0 + \beta y$. The present study shows that varying the initial y-position at $f_0 = 0$ is dynamically equivalent to varying f_0 at constant initial y-position.

Several workers have investigated theoretically the motion of vortices on a β-plane. Of particular relevance here is the analytical study of Llewellyn-Smith (1997) on the evolution of non-isolated vortices (the monopole used in the present paper is non-isolated) on a β-plane. Similar related studies have been performed by e.g. Sutyrin and Flierl (1994), Reznik and Dewar (1994) and Korotaev and Fedotov (1994). One of the results of these studies is that the difference in magnitude of the vorticity gradient across the vortex and the background vorticity gradient due to the β-effect determine the trajectory of the vortex. It is possible that these analytical approaches could be extended to incorporate the combined effect of a bottom topography and the disturbance in the overall background vorticity due to the β-effect, though such an analytical treatment falls outside the scope of the present paper. Instead, the attention is focussed here on the results of numerical experiments of a set of interaction processes and the classification of the possible outcome of these interactions.

The remainder of this paper is organised as follows. The numerical model is outlined in Section 2 and the motion of a monopole on a β-plane without topography is briefly addressed in Section 3. Sections 4 and 5 present the results of simulations in which the monopole encounters a north–south ridge and trough, respectively, and some concluding remarks are formulated in Section 6.

2. The numerical model

This section describes in brief the numerical method (see VGD for details) and introduces the monopole and topography used in the simulations.

2.1. The governing equations

In a Cartesian (x, y, z) frame with unit vectors $(\boldsymbol{i}, \boldsymbol{j}, \boldsymbol{k})$, assuming that vertical motions induced by a topography are much smaller than the horizontal motions ($w \ll u, v$, with $\boldsymbol{v} = (u, v, w)$ the relative velocity of the flow), conservation of mass for an incompressible fluid is given by

$$\nabla \cdot \boldsymbol{v} = -\frac{1}{H}(\boldsymbol{v} \cdot \nabla)H, \tag{1}$$

where $H(x, y)$ is the fluid depth. It is convenient to introduce a *potential streamfunction* ψ_p, defined as

$$\begin{cases} Hu = \partial\psi_p/\partial y \\ Hv = -\partial\psi_p/\partial x \end{cases} \quad \text{or} \quad H\boldsymbol{v} = \nabla \times \boldsymbol{k}\psi_p = \nabla\psi_p \times \boldsymbol{k}. \tag{2}$$

With this definition, which satisfies Eq. (1), the two-dimensional (2D) Navier–Stokes equation in the vorticity–streamfunction formulation reads

$$\frac{\partial\omega}{\partial t} + J(\omega_p, \psi_p) = \nu\nabla^2\omega, \tag{3}$$

where ν is the kinematic viscosity, J the Jacobian operator (describing the non-linear advection effects), and ω the *relative vorticity*. The *potential vorticity* ω_p is defined by

$$\omega_p = \frac{\omega + f}{H}, \tag{4}$$

where f is the Coriolis parameter, describing the latitudinal variation of the vertical component of the Earth's angular velocity Ω_s. Expanding f around a reference latitude ϕ_0 for a sphere of radius R_s leads to (e.g. Van Heijst, 1994)

$$f = f_0 + \beta y + \mathcal{O}(y^2), \tag{5}$$

in the so-called β-plane approximation used in this paper. In Eq. (5), the local north coordinate is y and

$$f_0 = 2\Omega_s \sin\phi_0, \quad \beta = 2\Omega_s \cos\phi_0/R_s. \tag{6}$$

If Eq. (3) is made dimensionless using a typical length scale L_0 and a typical time scale T_0, the familiar Reynolds number Re appears as

$$\mathrm{Re} = \frac{L_0^2/T_0}{\nu} = \frac{\Gamma_0}{\nu}, \tag{7}$$

where Γ_0 is a typical scale for the circulation of the vorticity distribution. In what follows, all typical scales are, by choice, set equal to unity, so that the Reynolds number, in effect, is $\mathrm{Re} = 1/\nu$, and all quantities are given in dimensionless units (see VGD). This implies that a vortex with a translation velocity of 2, say, travels 2 length units in 1 time unit. The default fluid depth, away from any topography, is $H = 1$.

The relation between vorticity and streamfunction is given by what can be denoted the *modified Poisson equation*:

$$H\omega = -\nabla^2\psi_p + \frac{1}{H}(\nabla H \cdot \nabla\psi_p), \tag{8}$$

which reduces to the regular Poisson equation $\omega = -\nabla^2\psi$ for a uniform fluid depth (with ψ the regular streamfunction).

Eqs. (3) and (8) form the set of equations solved by the numerical method for given $H=H(x, y)$, f_0 and β, starting from an initial vorticity distribution $\omega(x, y, t = 0)$.

2.2. The numerical method

The numerical method used is a finite difference method that solves Eqs. (3) and (8) on a rectangular grid in a rectangular domain in the x, y-plane. The time evolution in Eq. (3) is computed with an explicit third-order Runge–Kutta scheme, the viscous term $\nu\nabla^2\omega$ with a Crank–Nicolson scheme and the non-linear term $J(\omega_p, \psi_p)$ with the Arakawa scheme. The use of the Arakawa scheme (Arakawa, 1966) guarantees, on the one hand, that in the inviscid case energy, enstrophy and skew symmetry are conserved, and, on the other hand, that the computation has a high degree of stability. Eq. (8) is solved with a multigrid method by a routine from the NAG Library, which limits the number of grid cells to 2^n ($n = 1, 2, 3, \ldots$) in either direction.

The possible effects of the boundaries of the domain are minimised by using a free-slip condition on the boundaries (which means that the boundary is a streamline along which the fluid can flow freely) and by using a domain that is much larger (see below) than the diameter of the monopolar vortex used for the interaction studies.

2.3. The computations

For the study of the interaction of a monopole with a topographic ridge, a Bessel monopole is used. This is a monopolar vortex of Bessel type with a vorticity distribution given by

$$\omega = \begin{cases} \dfrac{(kR)\Gamma}{2\pi R^2 J_1(kR)} J_0(kr), & r \leqslant R, \\ 0 & r \geqslant R, \end{cases} \tag{9}$$

where r is the radial distance to the centre of the vortex, R its radius, and Γ its strength or circulation. J_0 and J_1 are Bessel functions of the first kind and $kR \approx 2.4048$ is the first non-zero root of J_0. The maximum of vorticity is located at the centre of the monopole, where J_0 equals unity. (The vortex given by Eq. (9) is an exact, stationary solution of the inviscid vorticity equation without topography and a background rotation independent of location – i.e. Eq. (3) with $\nu = 0, H = 1$ and $f =$ constant – in an infinite domain, satisfying the linear relationship $\omega = k^2\psi$.)

This monopole moves through the domain as a result of the β-effect (see Section 3) and encounters a smooth, cosine-shaped ridge along the y-axis, such that the fluid depth is given by

$$H = \begin{cases} 1 - A\cos(x\pi) - A, & -1 < x < +1, \\ 1, & \text{elsewhere}, \end{cases} \tag{10}$$

with the maximum height of the ridge (at $x = 0$) being $2A$ and the width at its foot being 2. The height of the ridge is varied, where negative A-values obviously give a trough rather than a ridge. Since the motions are assumed to be 2D, the absolute value of A cannot be too large.

The Bessel monopole is initialised with $\Gamma = +4$ and $R = 0.5$. This monopole is thus cyclonic (anti-cyclonic) on the northern (southern) hemisphere, and it moves to the northwest (see

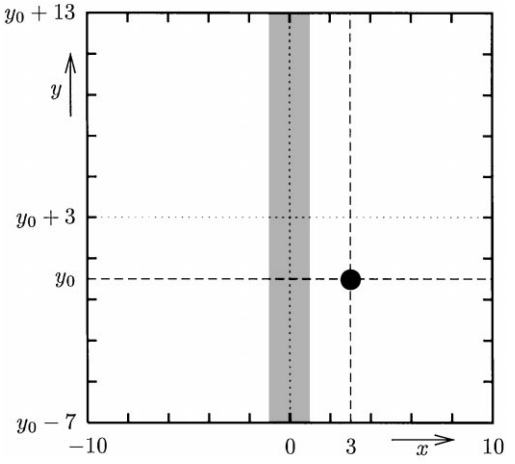

Fig. 1. Sketch of the initial situation with a cyclonic Bessel monopole ($\Gamma = 4, R = 0.5$) at ($x_0 = 3, y_0$) and the cosine-shaped ridge along the y-axis (shaded region), given by Eq. (10).

Section 3). The monopole's initial location is $(x_0 = +3, y_0)$, where y_0 is varied for $f_0 = 0$ and ascribing the value $y_0 = -3$ for non-zero f_0. If y_0 is varied, the computational domain moves also in the y-direction to minimise the boundary effects, as sketched in Fig. 1. The position $y_0 = -3$ is chosen as default value because if the monopole starts from $(+3, -3)$ and travels to the northwest, it passes the line $y = 0$ (the reference latitude of the Coriolis parameter, where $f = f_0$) at about $x = 0$ if there is no topography. Thus, $y_0 = -3$ may be regarded as a symmetry case for assessing topographic modifications to the flow. Note that from Eqs. (5) and (6) it follows that if $f_0 = 0$ the equator is the line $y = 0$.

Initially, a passive tracer is placed at the centre of the monopole, the location of the maximum $\omega_{\max}$ of vorticity. If the monopole moves on a pure β-plane this tracer stays at $\omega_{\max}$ and the tracer can be used to track the vortex. Any interaction with the topography, however, can deform the monopole so much that $\omega_{\max}$ moves away from the tracer. Likewise, if the deformation is very strong (or the vortex has decayed due to viscous effects), then $\omega_{\max}$ may be located near one of the boundaries or at the topography, even if there still is a vortex to be seen. The location and value of $\omega_{\max}$ are only determined at grid points — whereas a tracer can move between grid points — and a plot of $\omega_{\max}$ necessarily shows steps from grid point to grid point. This obscures the effects being studied and, therefore, a running average over 20 time steps is used in graphs (like Fig. 4) of $\omega_{\max}$.

The computational domain measures 20×20 length units and is divided in 256×256 grid cells (generally only a part of this domain is shown in the graphs). The influence of the size of the domain on the vortex' evolution has been subject to a previous sensitivity analysis (see VGD) and a 20×20 domain has been shown to be sufficiently large to neglect boundary effects. The values $\Delta t = 0.05$, $\beta = 0.3$ and $\mathrm{Re} = 1000$ are taken for all simulations presented here. All runs end at $T = 50$, unless the fate of the monopole is still uncertain, in which case the run is continued until $T = 75$ or 100.

3. Motion of a monopole on a β -plane

A monopolar vortex like the Bessel monopole (9) has a net angular momentum, so it rotates about its centre. It has no net linear momentum, so it does not move in an infinite domain. If placed in a finite domain with free-slip boundaries, however, the monopole moves along a closed trajectory around the centre of the domain, since it "feels" its images in the boundaries, as shown by Van Geffen et al. (1996); the further away the monopole is from the boundary, the slower it moves.

On a β-plane the situation is essentially different. As the monopole rotates, fluid parcels are advected around it and conservation of potential vorticity (assuming for a moment that the fluid is inviscid) leads to the creation of relative vorticity. The result is that the monopole will move, to the northwest (southwest) for a cyclonic (anti-cyclonic) monopole on the northern hemisphere (see e.g. Van Heijst, 1994; Reznik and Dewar, 1994; Llewellyn-Smith, 1997). The monopole does not move along a straight path: as it moves, it leaves vorticity behind in the form of Rossby waves and the monopole interacts subsequently with this vorticity. This secondary β-induced vorticity field, by some authors named beta-gyres, has a dipolar-like fluid motion and forces the vortex to move along the dipole axis. This axis rotates because of the pattern in the vortex circulation and this leads to rather complex trajectories with bends and kinks (see, for instance, the dotted curve in Fig. 9). The β-induced motion is much stronger than the motion induced by the boundaries in the 20×20 domain, as shown by VGD.

For the motion of the monopole on the β-plane without topography, the value of the constant f_0 in the Coriolis parameter is unimportant, as can be seen from Eq. (3): the Coriolis parameter f only appears in the derivatives of the Jacobian operator. Similarly, it does not matter from what initial y-position (y_0) the monopole starts, since $f = \beta y$ at another y_0 simply means that a constant is added to f. If the fluid depth H is a function of the position, however, the values of both f_0 and y_0 influence the evolution of the monopole, as shown below.

4. The monopole encounters a north–south ridge

In the simulations described by VGD for a cyclonic monopole encountering a ridge along the y-axis [given by Eq. (10)] as it moves to the northwest, the monopole starts from the initial y-position $y_0 = -3$, and the constant part of the Coriolis force is $f_0 = 0$. As summarised in the Introduction, the ability of monopole to cross the ridge is controlled significantly by the amount of positive potential vorticity acquired at its (north)west side, for non-trivial cases of finite-height topography.

This can be seen in Fig. 2, which shows a time sequence of contours of potential vorticity ω_p for a ridge with $A = 0.20$. The monopole reaches the foot of the ridge at about $T = 15$ and ascends the ridge somewhat. It then travels north along the ridge, i.e. to the region of positive potential vorticity in the undisturbed flow (cf. Fig. 11). At about $T = 25$ the vortex has only positive potential vorticity at its northwest side and the maximum of vorticity crosses the top of the ridge. The deformations in the shape of the monopole caused by this ridge are relatively large and the vortex is seen to disintegrate subsequently into two pieces. The front part, containing the maximum of vorticity, becomes a more or less circular monopole that descends and eventually leaves the ridge. The trailing part decays due to viscous effects before it can leave the ridge. After about $T = 22$, because of the deformations of the monopole, the tracer is no longer located at the maximum of vorticity: the tracer moves across

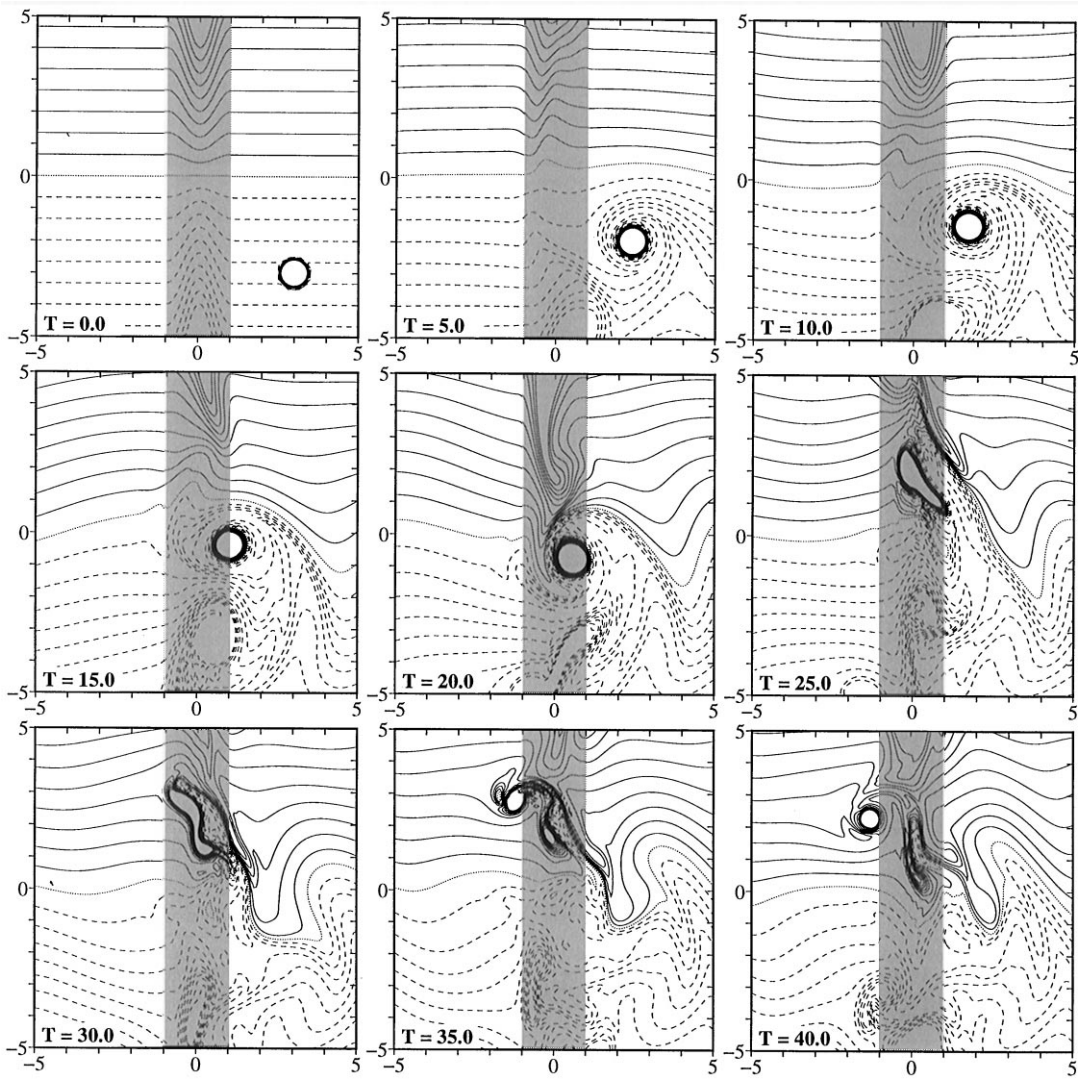

Fig. 2. Contours of potential vorticity on the x,y-plane of a Bessel monopole, initially at $(3,-3)$, encountering a ridge given by Eq. (10) with $A=0.20$ (shaded region) and $f_0=0$. Contours are drawn at intervals of 0.2 in the range $[-2.0;2.0]$; positive contours are solid, negative dashed, and the zero contour is dotted. At $T=0$ the zero contour coincides with the equator; since $f_0=0$ this is at $y=0$. Note that in this and following plots only the central part of the computational domain is shown.

the top of the ridge at $T=25$ and stays in the front part of the vortex, where it circles around $\omega_{\max}$ as the vortex travels on.

The point to address is the possible influence of another initial y-position y_0 at $f_0=0$, and of a non-zero f_0 at $y_0=-3$ on the monopole's evolution. These two cases are equivalent, as can be seen by equating their Coriolis parameters:

$$f_0+\beta y_0=f_0^*+\beta y_0^*, \tag{11}$$

where the terms on the left represent the case of variable y_0 and the terms on the right the case of non-zero f_0. Hence in Eq. (11): $f_0 = 0$ and $y_0^* = -3$, so that

$$f_0^* = \beta(3 + y_0), \tag{12}$$

which has been confirmed numerically. This implies that both cases can be inter-changed at will, where Eq. (12) gives their relationship, with $\beta = 0.3$ for the simulations presented in this paper. The value of y_0 is changed in steps of 2, which is thus equivalent to f_0^* being changed in steps of 0.6.

4.1. A ridge with height $A = 0.20$

The top-left panel in Fig. 2 shows that the contours of potential vorticity ω_p of the β-effect (βy) are parallel to the x-axis. These contours are deformed above the topography: they are squeezed towards the equator, which has $\omega_p = 0$ (dotted line; since $f_0 = 0$ the equator is at $y = 0$). For $y_0 = -3$ (or equivalently $f_0^* = 0$) the monopole crosses the ridge, despite some deformation, as shown in Fig. 2 and discussed above. Placing the monopole initially more to the north — equivalent to giving f_0^* a positive value — brings the monopole closer to, and finally into the region with only positive ω_p.

For $y_0 = -3$ it is found by VGD that the maximum of vorticity ω_{max} is able to cross the top of a finite-height ridge only after the monopole has gathered sufficient positive ω_p at its northwest side. In the present study, for $y_0 = -1$ (or $f_0^* = 0.6$) this is also the case, as the monopole starts (as for $y_0 = -3$) in a region of negative ω_p. For this case, however, the deformation of the monopole is so strong that at $T = 41$ the tracer is no longer at ω_{max}; in fact, ω_{max} is no longer located at the centre of the vortex.

More dramatic is the case with $y_0 = +1$ (or $f_0^* = 1.2$), for which Fig. 3 shows a time sequence of contours of ω_p and for which the monopole starts off completely surrounded by positive ω_p. The potential vorticity field in this case causes the tracer to clearly separate from ω_{max} around $T = 22$, though by only a relatively small amount, as can be seen in Fig. 4. The deformation continues and after about $T = 40$ the tracer is really away from ω_{max}: the vortex is fully disintegrated.

For $y_0 = +1$, the case discussed above, the monopole is obviously destroyed by the topographic interaction. For the $y_0 = -1$ counterpart case discussed earlier, the fate of the vortex is less clear, since at $T = 50$ there still is a vortex visible. Fig. 5 shows contours of ω_p of this case, with the position of the tracers being marked by a white circle: the tracer remains at the centre of the decaying vortex. The maximum of vorticity, however, is after $T = 41$ located outside the vortex (see the figure caption), indicating that the monopole is trapped on the ridge and decays there due to viscous effects.

For initial positions more northerly than $y_0 = +1$, the deformation of the monopole is qualitatively similar to the case $y_0 = +1$: the computations show that the tracer is away from ω_{max} at about $T = 22$–24 and after about $T = 40$ a vortex is no longer visible. In these cases ω_{max} is often located near one of the boundaries or somewhere on the ridge, but not at the position of the tracer.

Conversely, placing the monopole initially further to the south than $y_0 = -3$ (equivalent to giving f_0^* a negative value) means that the vortex is initially surrounded by progressively stronger negative values of ω_p. In these cases, crossing the ridge is more and more inhibited by the ridge-induced vorticity. For example, the model results show that for $y_0 = -5$ (or $f_0^* = -0.6$) this tendency is strengthened, relative to the $y_0 = -3$ case (Fig. 2). As the monopole approaches and encounters the ridge, negative vorticity is generated to the south of the vortex. The combination of this advected topography-induced vorticity and the monopole generates a dipolar-like structure which then tends

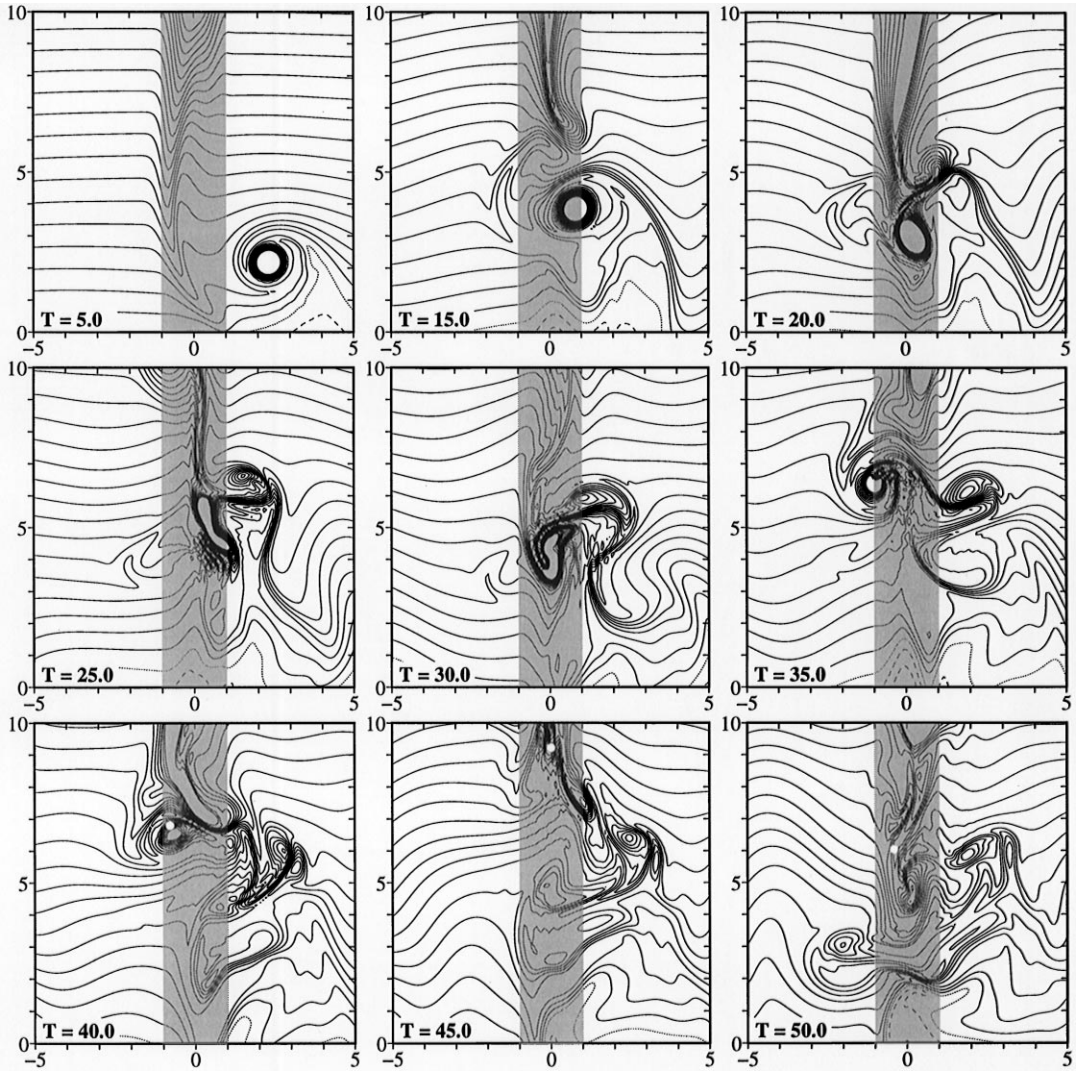

Fig. 3. Contours of potential vorticity on the x,y-plane of a Bessel monopole, initially at $(3,+1)$, encountering a ridge given by Eq. (10) with $A = 0.20$ (shaded region) and $f_0 = 0$. Contours as in Fig. 2 in the range $[-1.0; 4.0]$. A small white circle (0.25 length units in diameter) shows in the last three panels the position of the tracer, which is at the ridge then; cf. Fig. 4.

initially to move away from the ridge. This dipolar structure is, however, relatively weak and the monopole component is soon free again to — with some delay — actually start climbing the ridge. At $T = 50$ the maximum of vorticity has still not crossed the summit, obstructed as it is by the negative vorticity above the ridge, northwest of the vortex. Continuing the computation beyond $T = 50$ shows that $\omega_{\max}$ does leave the ridge eventually after crossing the summit at about $T = 60$ and having undergone strong deformations but no disintegration. The vortex then descends from the ridge and travels to the northwest again.

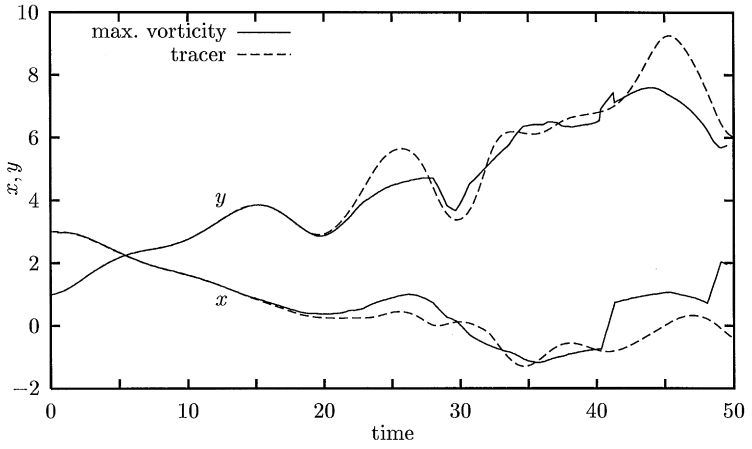

Fig. 4. The x- and y-position of the maximum of vorticity (solid line) and the tracer (dashed line) as function of time of the monopole of Fig. 3.

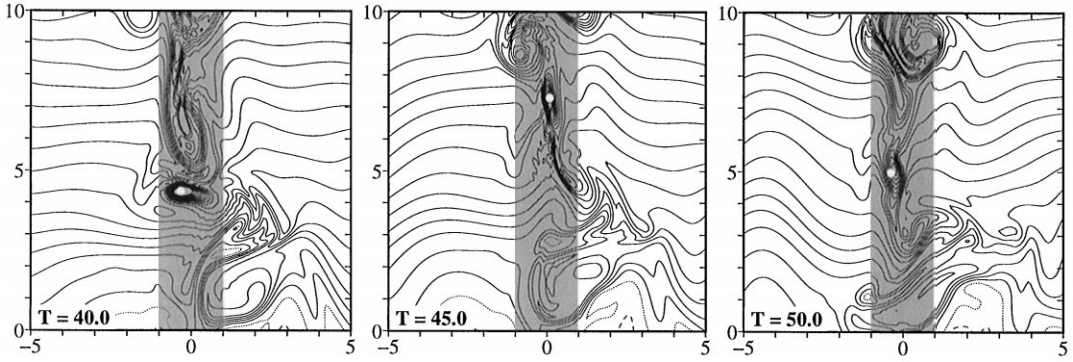

Fig. 5. Contours of potential vorticity on the x, y-plane of a Bessel monopole, initially at $(3, -1)$, encountering a ridge given by Eq. (10) with $A = 0.20$ (shaded region) and $f_0 = 0$. Contours as in Fig. 2 in the range $[-1.0; 4.0]$. A small white circle (0.25 length units in diameter) shows the position of the tracer, which is at the ridge. At the times shown, the maximum of vorticity is located at the tracer, at $(-0.9, 8.6)$ and at $(0.9, 9.2)$, respectively.

With the monopole initially located further to the south, for example, for $y_0 = -7$ the process is initially the same as described above for $y_0 = -5$, but the effect of the ridge-induced vorticity is stronger than in the latter case: the dipolar-like structure formed by the negative vorticity generated at the ridge and the monopole is more coherent and clearly moves away from the ridge. The result is that the monopole rebounds from the ridge, without $\omega_{\max}$ having reached the foot of the ridge. Fig. 6 shows a time sequence of contours of ω_p for this case and Fig. 7 shows the monopole's trajectory: the tracer remains at $\omega_{\max}$ fairly well during the rebound. For even lower values of y_0 the monopole also rebounds from the ridge; the position of $\omega_{\max}$ does not approach closer to the ridge than $x \approx 1.7$ and the tracer follows $\omega_{\max}$ well.

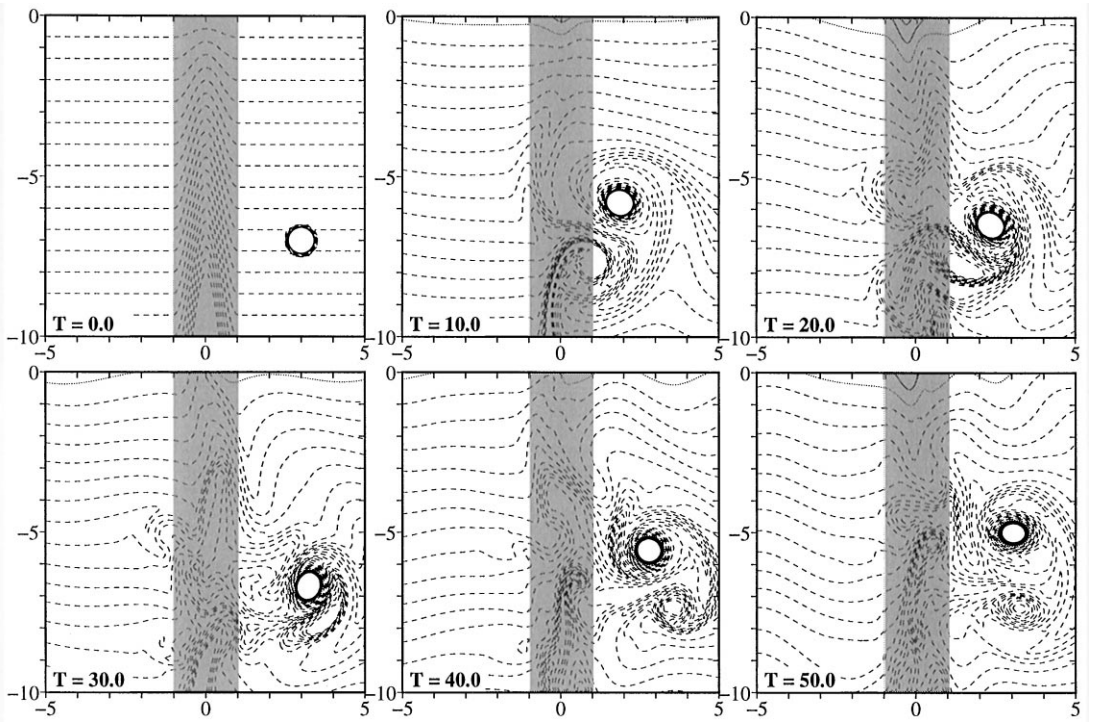

Fig. 6. Contours of potential vorticity on the x, y-plane of a Bessel monopole, initially at $(3, -7)$, encountering a ridge given by Eq. (10) with $A = 0.20$ (shaded region) and $f_0 = 0$. Contours as in Fig. 2 in the range $[-4.0; 1.0]$.

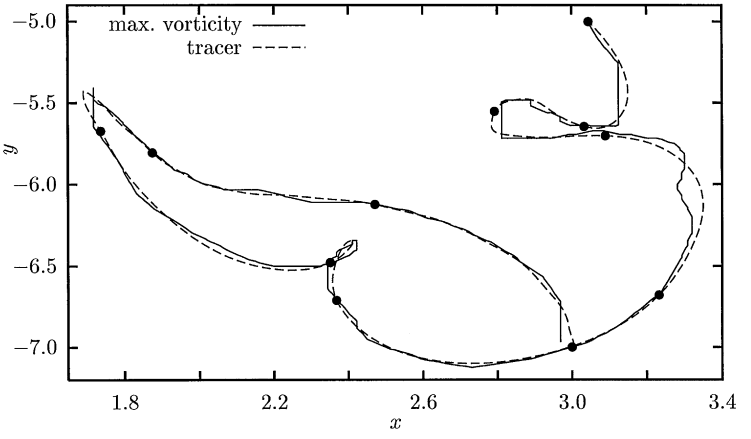

Fig. 7. Trajectory of the maximum of vorticity (solid line) and the tracer (dashed line) of the monopole of Fig. 6. Black dots mark the position of the tracer at intervals of $\Delta T = 5$.

Obviously, when the rebounded monopole has shed some of the negative vorticity with which it formed a dipolar-like structure (which prevented the monopole from reaching the ridge in the first attempt), the monopole will again move to the northwest due to the β-effect. For the case shown in Figs. 6 and 7, for example, this is going to happen after $T = 50$, when the dipolar-like structure has disintegrated (last panel in Fig. 6). In consequence, the monopole will encounter the ridge again, but somewhat further to the north than initially. In this circumstance, the monopole has by then become weaker and larger in lateral size due to viscous effects, so it is not clear whether the monopole will be able to cross the ridge in the subsequent encounter. (This point has not been addressed any further, as the first encounter with the ridge is the subject of the present study.)

In summary, the fate of the monopole due to the interaction with the ridge in question can be classified arbitrarily in four categories:

- 'd' for destroyed: the ridge deforms the monopole so much that the vortex is fully disintegrated;
- 't' for trapped: the monopole stays on (or very close to) the ridge and decays due to viscous effects;
- 'c' for crossed: the monopole manages to cross the ridge, maintaining its integrity, though with the possible loss of a part of the vortex;
- 'r' for rebounded: the topography prevents the monopole from crossing the ridge on first encounter.

Table 1 gives the fate of the monopole for varying y_0 (or, equivalently, for varying f_0^*) for the ridge with $A=0.20$ discussed above. The time T_f listed marks the time at which $\omega_{\max}$ moves away from the tracer. If that does not happen before the run ends, the end-time of the run is given between brackets.

4.2. Ridges with other heights

Table 1 summarises the corresponding interaction results for all ridges investigated in the present study, including three cases for which the value of A is lower than the $A = 0.20$ value described

Table 1
The fate of a Bessel monopole encountering a north–south ridge along the y-axis, given by Eq. (10), starting from $(3, y_0)$ at $f_0 = 0$ (in which case the equator is at $y = 0$). The second column gives the equivalent f_0^* value according to Eq. (12), where the monopole is initially at $(3, -3)$. For a description of the classification of the monopole's fate and the meaning of T_f, see the end of Section 4.1

		$A = 0.20$		$A = 0.15$		$A = 0.10$		$A = 0.05$	
y_0	f_0^*	Fate	T_f	Fate	T_f	Fate	T_f	Fate	T_f
+7	3.0	d	23.8	d	22.7	d	53.1	d	59.3
+5	2.4	d	22.4	d	30.7	d	60.5	t	58.5
+3	1.8	d	23.2	d	43.9	t	72.3	t	59.0
+1	1.2	d	22.3	d	58.8	d	54.2	c	62.0
−1	0.6	d/t	40.9	d	53.0	c	58.1	c	(50)
−3	0.0	c	(50)	c	(50)	c	(50)	c	(50)
−5	−0.6	c	(75)	c	(50)	c	(50)	c	(50)
−7	−1.2	r	(50)	r	(50)	c	(50)	c	(50)
−9	−1.8	r	(50)	r	(50)	t	70.9	c	(50)
−11	−2.4	r	(50)	r	(50)	r	(50)	c	(75)
−13	−3.0	r	(50)	r	(50)	r	(50)	t	69.3

in the previous section. [Values larger than $A = 0.20$ are not acceptable within the assumption of 2D motions made in the model (Section 2).] The main conclusion, not surprisingly, is that a lower height has a less dramatic effect on the monopole's evolution (under otherwise-identical conditions), though it is noted that such effects of varying the ridge height are not linear. Likewise, the form of the interaction is controlled strongly by the value of y_0, i.e. by the form of the undisturbed potential vorticity field associated with the ridge.

With regard to the outcome of the interaction, it is noted that for sufficiently high values of ridge height A, the effects of further increases in A are weak. For example, a ridge with $A = 0.20$ exerts essentially the same qualitative effects upon the monopole as the ridge with $A = 0.15$, for both positive and negative values of y_0. In the latter regard, note that for $y_0 \leqslant -7$, for example, the 'r' flow type classification for the two A-values look alike, except for some differences in the trajectories associated with the precise nature of the interaction between the monopole and the ridge-induced vorticity: there is a clear rebound of the monopole against the foot of the ridge in both A-values. Even for the cases $y_0 = -3$ and -5, where the monopole crosses the ridge, the effects of increasing the value of A from 0.15 to 0.20 are not significant for either the general deformation of the vortex or the fate of the tracer (which remains on $\omega_{\max}$ for all times shown). For all positive values of y_0, the only effect of increasing the ridge height from 0.15 to 0.20 is a somewhat stronger monopole deformation (though with ultimate disintegration ('d') in both cases) and a correspondingly shorter survival time with the latter topography.

As the value of A is reduced further below $A = 0.15$, the effects of changing ridge height become more pronounced, both qualitatively and quantitatively. For example, for $y_0 = -9$, reducing the value of A from 0.15 to 0.10 and finally to 0.05 results in a transition of respective flow types from a rebounded monopole to a trapped monopole and finally to a crossing of the ridge by the monopole. For the lowest ridge case studied ($A = 0.05$), no rebound of the incident monopole is observed within the full y_0-range ($+7 \rightarrow -13$) investigated.

A similar dependence upon the value of A is illustrated in the time sequence of ω_p for a ridge of height $A = 0.10$ shown in Fig. 8 and the associated plot of the monopole trajectory in Fig. 9. For this case, the value of y_0 is -7, as in the counterpart sequence for $A = 0.20$ in the earlier Figs. 6 and 7. Comparisons between Figs. 6 and 8 show that the reduction in ridge height alone has resulted in a change in flow type, with the lower ridge allowing passage over the topography by the monopole. Such a difference in flow behaviour between the two ridge heights is shown dramatically in the differences in the respective trajectory plots of Figs. 7 and 9. In addition, however, to these (not-unexpected) quantitative differences between topographies having different ridge heights, a crucial revelation of Fig. 8 alone is that (contrary to the findings of VGD for $f_0 = 0$) the incident monopole is able to cross the ridge even if it does not have positive potential vorticity ω_p at its northwest side.

Thus, the present study, in which f_0 is essentially varied, evidently shows that the existence of a zone of positive potential vorticity to the northwest of the distorted vortex is neither necessary nor sufficient to determine whether the vortex can cross the ridge. Rather, it is the form of the undisturbed potential vorticity contours associated with the ridge (see later) that exerts the crucial influence upon the monopole's motion across the ridge. For low ridges, the deformation of the pure β-plane vorticity contours is relatively weak, leading to a weaker ridge-induced deformation opposing the crossing of the ridge by the monopole. This property can be seen clearly (Table 1) from the results of the computations for $A = 0.05$ (the lowest ridge

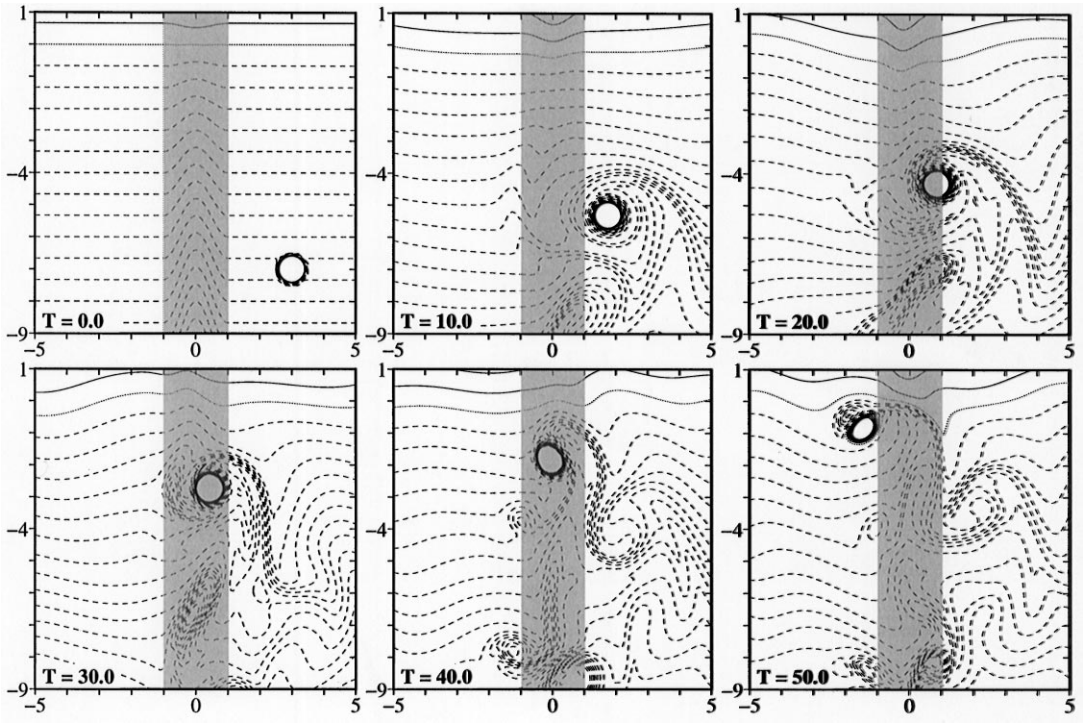

Fig. 8. Contours of potential vorticity on the x, y-plane of a Bessel monopole, initially at $(3, -7)$, encountering a ridge given by Eq. (10) with $A = 0.10$ (shaded region) and $f_0 = 0$. Contours as in Fig. 2 in the range $[-4.0; 1.0]$.

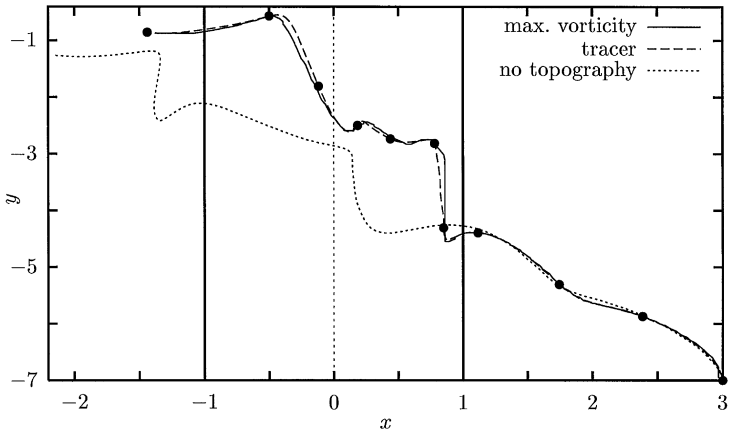

Fig. 9. Trajectory of the maximum of vorticity (solid line) and the tracer (dashed line) of the monopole of Fig. 8. Black dots mark the position of the tracer at intervals of $\Delta T = 5$. The dotted line shows the monopole's path in the absence of a topography. Thick vertical lines in this and following plots indicate the edges of the ridge.

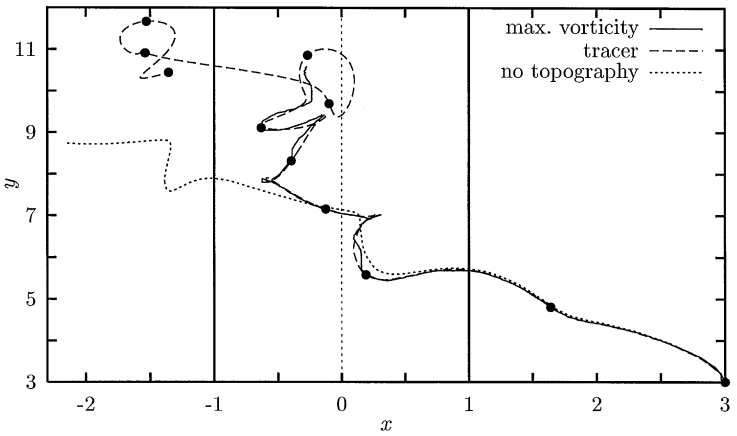

Fig. 10. Trajectory of the maximum of vorticity (solid line; until $T = 59$) and the tracer (dashed line) of a monopole, initially at $(3, 3)$, encountering a ridge given by Eq. (10) with $A = 0.05$ and $f_0 = 0$. Black dots mark the position of the tracer at intervals of $\Delta T = 10$. The dotted line shows the monopole's path in the absence of a topography.

considered): the monopole can cross such a ridge for all $f_0^* < 0$ cases, except for the lowest y_0-position.

For non-negative values of f_0^*, interactions of the monopole with the lowest ridge ($A = 0.05$) can result in the decay of the monopole at the ridge rather than disintegration. When the maximum of vorticity is no longer at the location of the tracer (i.e. for $T > T_f$), there is still a vortex to be seen. Fig. 10 illustrates the trajectory of such cases; for this example ($f_0^* = +1.8$) the tracer is near the summit of the ridge until about $T = 70$, after which it descends to the western side and after about $T = 80$ remains near the location $x = -1.5$, $y = 11$. The maximum of vorticity, meanwhile, is located near the southwestern corner of the domain after $T = 59$.

The case study examples presented above expose the limitations of interpreting the crossing of a given ridge solely in terms of the existence of positive potential vorticity to the northwest of the advecting monopole. Rather, they point to the importance in this regard of the undisturbed form of the potential vorticity contours associated with the topographic feature. For a given value of A, such contours are of course of different form for different values of y_0. Most significantly, the contours are also of different form for positive and negative topographies (ridges and troughs, respectively) of otherwise-identical amplitude $|A|$, suggesting that the motion of the monopole will be sensitive to the sign of the topography as well as the values of y_0 and A. The next section shows the results of computations designed to investigate this hypothesis.

5. The monopole encounters a north–south trough

Within the context of the above discussion, it is important to note that for negative values of A in Eq. (10), the contours of potential vorticity above the (trough) topography are widened, as opposed to being narrowed as for the counterpart contours above the ridge discussed in the preceding sections.

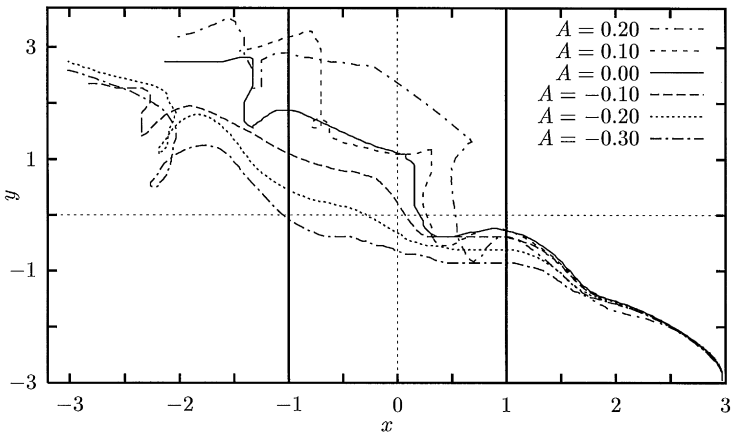

Fig. 11. Trajectories of the maximum of vorticity of a monopole, initially at $(3, -3)$, encountering a ridge or trough given by Eq. (10) with several heights A, including the no-topography case $A = 0$ (solid line). In all cases $f_0 = 0$.

As shown in the trajectory plots of Fig. 11, for the reference starting position $y_0 = -3$, the differences in the form of the potential vorticity contours for ridges and troughs having the same values of $|A|$ result in rather dramatic differences in the monopole's motion across the topography. For example, (i) for positive values of A, the monopole bends significantly further to the north than the negative A counterpart on the approach to the ridge, and (ii) the final displacement of the monopole after crossing the ridge is significantly further to the north with the ridge topographies than with the trough counterparts. Note that the cases shown in Fig. 11 are all characterised as a 'c' flow type for all positive values of A considered (see Table 1).

Further evidence of such differences in the behaviour of the monopole in its interaction with topography is presented in Fig. 12, where a time sequence of contours of ω_p is shown for a monopole encountering a trough of $A = -0.20$. Such an interaction can be compared directly with the sequence shown in Fig. 2, where the only difference in prescibed conditions from Fig. 12 is the difference in sign of A. Such comparisons show clearly that the degree of deformation caused to the monopole is significantly less when the topography is a trough instead of a ridge of the same amplitude $|A|$. A summary of the behaviour of the monopole for different trough depths and initial positions y_0 is given in Table 2, a table that can be compared directly with the corresponding ridge results presented in Table 1.

An important difference between a ridge and a trough is the effect of the topography upon the size and strength of the vortex that tries to cross it. This can be seen by writing Eq. (3) as

$$\frac{\mathrm{D}}{\mathrm{D}t}\left(\frac{\omega + f}{H}\right) = \nu\nabla^2\omega, \tag{13}$$

where $\mathrm{D}/\mathrm{D}t$ is the material derivative. Assuming for a moment that viscous effects are negligible while the vortex crosses the topography, $\omega_p = (\omega + f)/H$ is conserved according to Eq. (13). If f does not vary significantly when the monopole crosses the topography, then it follows that a monopole climbing a ridge weakens. At the same time it becomes larger in lateral extent due to conservation of mass inside the vortex (see also VGD, who show this in a number of cases). This makes it easier for the monopole to be deformed by the ambient vorticity field. On the other hand,

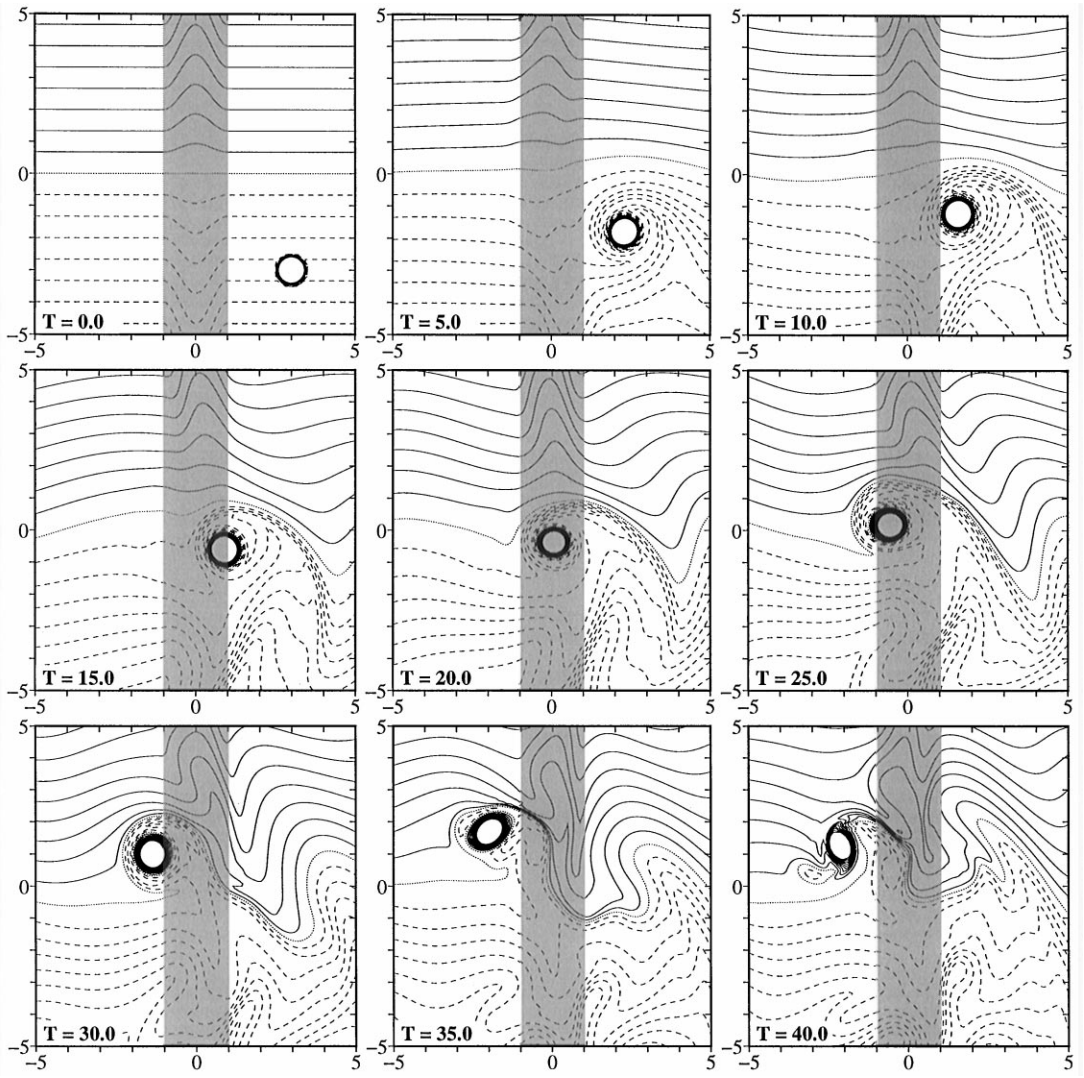

Fig. 12. Contours of potential vorticity on the x, y-plane of a Bessel monopole, initially at $(3, -3)$, encountering a trough given by Eq. (10) with $A = -0.20$ (shaded region) and $f_0 = 0$. Contours as in Fig. 2.

a trough, with its increase in fluid depth, causes the monopole to become stronger and smaller in lateral size. A vortex entering a trough is therefore less susceptible to deformations caused by topography-induced vorticity of a certain magnitude than a vortex which climbs a counterpart ridge.

Further interesting comparisons are revealed between trough and ridge effects for values of y_0 significantly less (i.e. more negative) than the value ($y_0 = -3$) in Fig. 12. For example, in Fig. 13 contours of ω_p are shown for $A = -0.20$ and $y_0 = -7$, a case comparable with the ridge in Fig. 6 having the same values of $|A|$ and y_0. In contrast to the case of the ridge (where the incident monopole is initially rebounded from the topographical barrier), the monopole in Fig. 13 first crosses

Table 2
As Table 1, but for a trough along the y-axis. In the cases marked with an asterisk, the monopole briefly enters the trough but leaves it again at the east side

		$A = -0.30$		$A = -0.20$		$A = -0.10$	
y_0	f_0^*	Fate	T_f	Fate	T_f	Fate	T_f
+7	3.0	r	(50)	r*	(50)	r	(50)
+5	2.4	r/d*	48.0	r	(50)	r*	(50)
+3	1.8	r	(50)	r	(50)	r*	(50)
+1	1.2	r*	(50)	r*	(50)	t	63.4
−1	0.6	c/d	39.2	c	(50)	c	(50)
−3	0.0	c	(50)	c	(50)	c	(50)
−5	−0.6	t/d	98.8	c	(50)	c	(50)
−7	−1.2	c	75.5	t	77.5	c	(50)
−9	−1.8	c/d	60.2	t	(100)	c	(75)
−11	−2.4	d	46.1	d	60.4	t	85.1
−13	−3.0	d	38.0	d	60.0	t/d	83.9

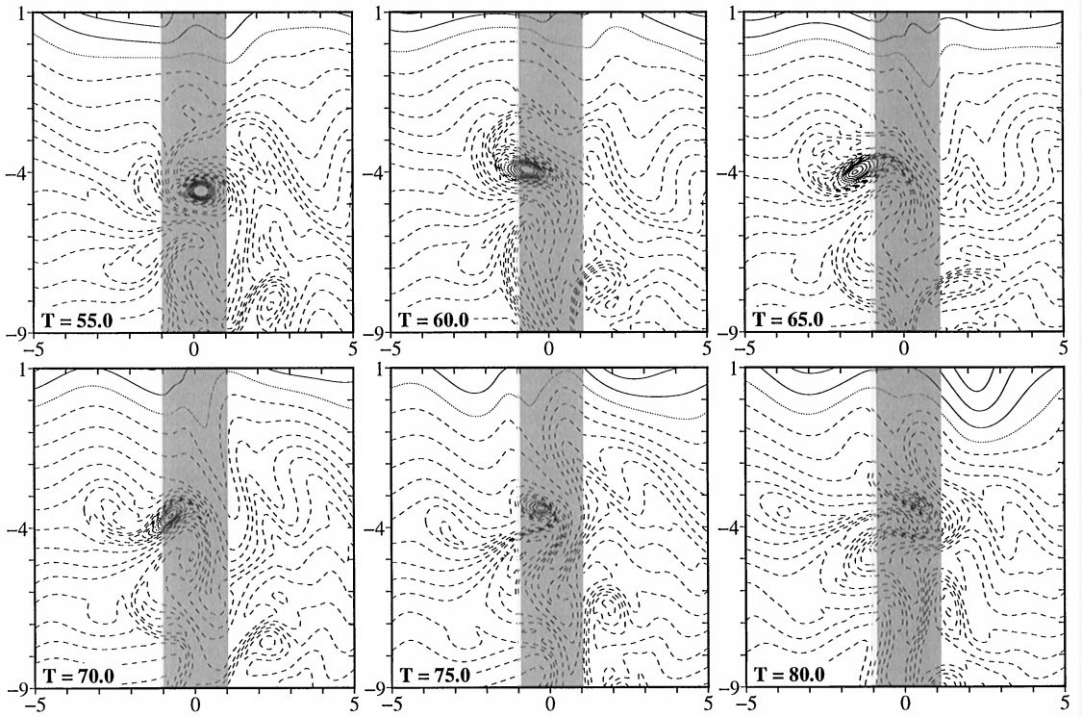

Fig. 13. Contours of potential vorticity on the x, y-plane of a Bessel monopole, initially at $(3, -7)$, encountering a trough given by Eq. (10) with $A = -0.20$ (shaded region) and $f_0 = 0$. Contours as in Fig. 2 in the range $[-4.0, 1.0]$.

the trough (at $T = 65$ both ω_{max} and the tracer are located close to $x = -1.5$), but the vortex returns eastward and, for this set of parameters, it stays inside the trough after about $T = 70$ and subsequently decays. Strictly, therefore, the monopole eventually becomes trapped ('t') by the topography, though by a mechanism different from the trapping process for the ridges. For the latter case, there is no prior crossing of the topographic feature before the trapping above the ridge occurs.

For the cases typified by Fig. 13, the vorticity induced by the topography at the monopole's western side (and the subsequent formation of a secondary dipolar structure) plays an important role; for the cases shown, this induced vorticity is evidently sufficiently strong for the monopole to be redirected back into the trough. As indicated in Table 2, interactions between troughs and monopoles initially having positive values of y_0 are characterised by the so-called rebound ('r') flow types. As with the trapped ('t') case of Fig. 13, however, the rebound phenomenon occurs in some cases (marked with an asterisk in Table 2) as a secondary effect *after* the monopole has initially entered the trough. In this sense, there is a rather fundamental difference in behaviour between 'r' and 't' flow types for the ridge and trough topographies. For the trough cases in which such secondary rebounds are observed, the tracer and ω_{max} are seen to penetrate no closer to the bottom of the trough than about $x = +0.5$.

Figs. 14–16 show the effects of the deepest trough studied ($A = -0.30$) upon the evolution of the monopole for the successively higher values of y_0. For the lowest value of y_0 shown ($y_0 = -9$), the ambient vorticity field retains the monopole within the trough, where it disintegrates (see Fig. 14); prior to this stage, the vortex enters the trough at about $T = 15$ and stays near the bottom where it decreases in strength due to viscous decay, subject to shape deformations. Fig. 14 shows that at about $T = 50$, when ω_{max} is still near $x = 0$, the vortex is strongly deformed and has lost much of its initial monopole structure. The position of both ω_{max} and the tracer show the monopole's subsequent westward movement out of the trough to $x = -2.8$ at $T = 60$, before the position of ω_{max} moves away suddenly from that of the tracer to a location along the boundary. By then, a clear vortex containing the tracer has formed and, due to the ambient vorticity field configuration, this vortex remains not far from $x = -3$ as it decays. Computations show that after about $T = 85$ this vortex feature is indistinguishable from the ambient vorticity field.

For higher values of y_0 at the same depth ($A = -0.30$) of trough, the above behaviour is modified significantly. For example, with $y_0 = -1$ (see Fig. 15) the monopole initially crosses the trough,

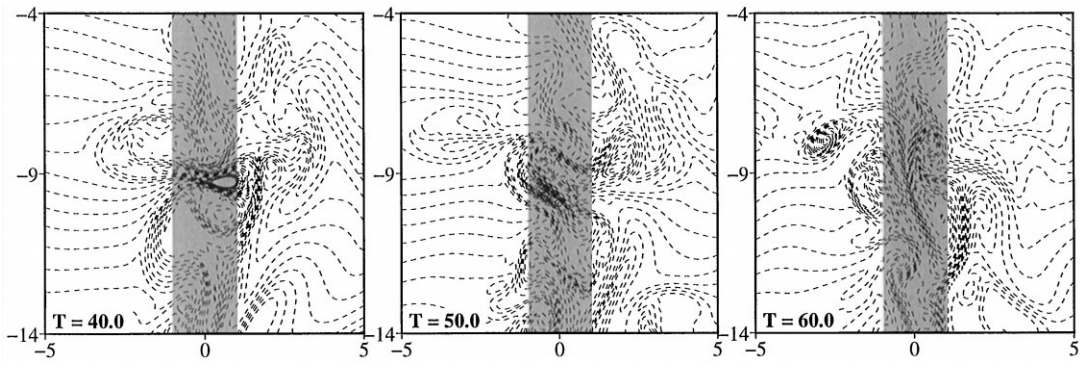

Fig. 14. Contours of potential vorticity on the x, y-plane of a Bessel monopole, initially at $(3, -9)$, encountering a ridge given by Eq. (10) with $A = -0.30$ (shaded region) and $f_0 = 0$. Contours as in Fig. 2 in the range $[-4.4; 0.6]$.

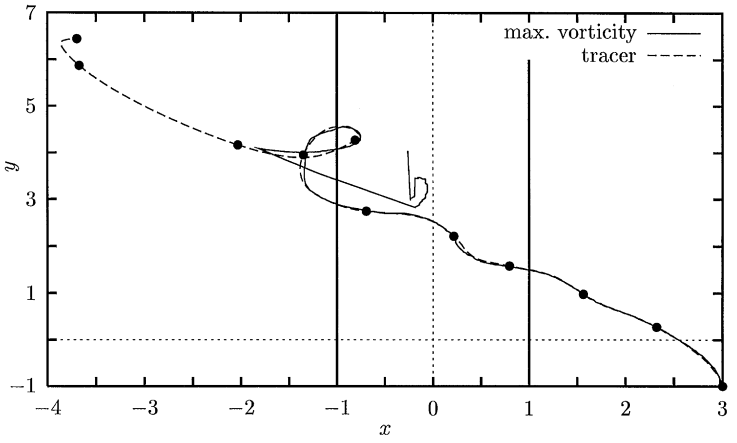

Fig. 15. Trajectory of the maximum of vorticity (solid line) and the tracer (dashed line) of a monopole initially at $(3,-1)$, encountering a ridge given by Eq. (10) with $A=-0.30$ and $f_0=0$. Black dots mark the position of the tracer at intervals of $\Delta T=5$.

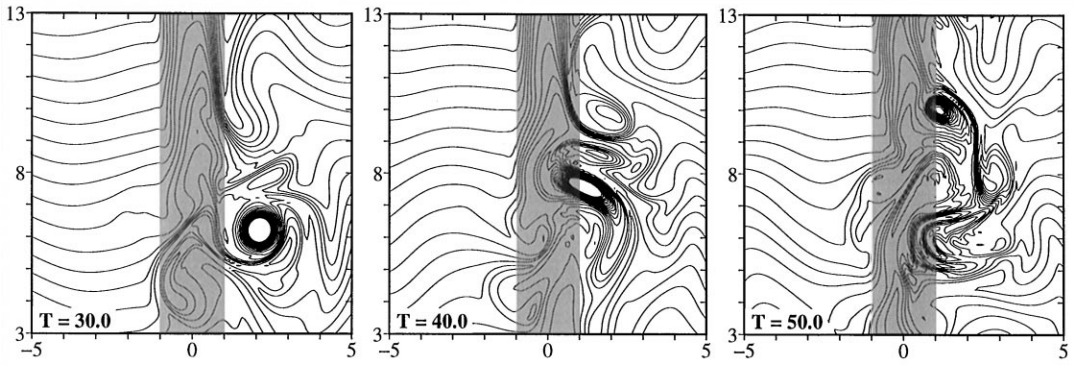

Fig. 16. Contours of potential vorticity on the x,y-plane of a Bessel monopole, initially at $(3,+5)$, encountering a ridge given by Eq. (10) with $A=-0.30$ (shaded region) and $f_0=0$. Contours as in Fig. 2 in the range $[0.6,5.0]$.

before being forced back into the trough by the deformed vorticity field. During this process (see Fig. 15), the position of both $\omega_{\max}$ and the tracer are near $x=-1$ at $T=25$–35; after about $T=40$ the position of $\omega_{\max}$ moves to the bottom of the trough while the tracer moves away to the northwest.

For the highest value of y_0 shown here ($y_0=+5$; see Fig. 16), the association between category 'd' and full disintegration of the vortex is inappropriate. The monopole is, of course, strongly deformed by the interaction with the potential vorticity field associated with deep trough. Computations show that the monopole approaches the trough until about $T=13$, when $\omega_{\max}$ and the tracer are located near $x=-1.7$. The monopole then moves away to the east, performs a few loops and returns to the trough for a second encounter after $T=30$. As Fig. 16 shows, after about $T=40$ the tracer and $\omega_{\max}$ reach the eastern edge of the trough, but the monopole is then so strongly deformed that the

tracer leaves ω_{max} and starts circling around it, following ω_{max} into the trough, where it remains at about $x = +0.25$. After $T = 48$ the vortex with the tracer moves away from the trough again at the east side, leaving ω_{max} elsewhere in the domain.

6. Concluding remarks

A two-dimensional numerical model has been used to study the effect of a north–south oriented ridge or trough on the evolution of a monopolar vortex that moves to the northwest due to the β-effect. The principle objective of the study has been to investigate the effects of different initial north–south positions y_0 of the monopole on the interaction with the topography, in order to extend a previous study (Van Geffen and Davies, 1999 — here named VGD) in which such an interaction was studied for a fixed value of y_0. The present study has shown that varying the initial y_0-position of the monopole is dynamically equivalent to changing the value of f_0, the reference constant value in the Coriolis parameter $f = f_0 + \beta y$. (Note that the previous VGD study considered only $f_0 = 0$, and that here only changes in y_0 were considered since varying y_0 at $f_0 = 0$ produces the same effect dynamically as varying f_0 at constant y_0.)

A further objective has been to investigate the effect upon the vortex–topography interaction of the initial, undisturbed configuration of the potential vorticity field associated with the topography. Since positive (ridge) and negative (trough) topographies of otherwise-identical geometrical forms and dimensions have different potential vorticity configurations, differences are to be anticipated between the interactions of a given monopole with a ridge or trough. The focus of the study has been to determine the nature of these differences for different values of A, the amplitude of the topographic element, and y_0, the initial north–south location of the monopole.

The study has shown that all of the above factors are able to influence directly the type of flow that results from the interaction of the self-propelled vortex and the topographical element. Tables 1 and 2 (contained within Sections 4 and 5, respectively) have summarised the various characteristic flow types observed with ridge and trough topographies, respectively, and have demonstrated, in particular, the differences between such identifiable flow types for the positive and negative A values. The model shows that for different initial positions y_0 there are essentially four regimes for the fate of the monopole: it can be destroyed, trapped or rebounded by the topographic interaction, as well as being able to cross it. Furthermore, the fate of the monopole depends on the amplitude $|A|$ of the tropography: the lower the value of $|A|$, the easier (i.e. for a wider range of y_0-positions) can the monopole cross the obstruction.

Of particular relevance here has been the observation in VGD that for the same domain and the same initial conditions as the present study, a monopole initially located at a fixed reference position $y_0 = -3$ ($f_0 = 0$) was evidently able to cross a given ridge only if it had gathered sufficient positive potential vorticity ω_p at its northwest side. Though such a conclusion is trivially invalid for ridge and trough topographies having infinitessimal amplitudes A, the cases of finite-height ridge topography considered in VGD and the particular value of $y_0 = -3$ investigated therein suggest strongly that such a distribution of ω_p is associated with the passage over the ridge by the vortex. The present study, however, with varying values of y_0 (or, equivalently, varying f_0-values) has shown that the finding of VGD is incomplete in this regard and that the fate of the monopole is determined generally by the initial potential vorticity configuration above the topographic element. The sign of

the potential vorticity is of importance because it determines the details of the potential vorticity distribution above the topography.

The present study has confirmed the findings of VGD that as the monopole propagates towards the topography, the principal effect of the motion of the monopole is the distortion caused to the initially undisturbed vorticity contours by the generation of Rossby waves. As a result of subsequent interactions with this secondary vorticity, the so-called beta-gyres (e.g. Sutyrin and Flierl, 1994) are generated (see Section 3); the monopole's trajectory far from the topography consists of small-scale lateral deviations superimposed upon a straight line path. As the vortex encounters the topography, the topographically generated potential vorticity field is advected by the velocity induced by the vortex itself. Since the contours of potential vorticity in the presence of a north–south ridge or trough are not simply aligned in the east–west direction, the topographic beta-gyres induced by the advection process become significantly different from the counterpart beta-gyres associated with the β-plane motion in the absence of topography.

Moreover, as the results of the computations discussed in the present paper illustrate (see, for example, Figs. 2, 3, 6, 8, and 12), the shape of the initially undisturbed potential vorticity contours with topography present depends on (i) the value of y_0, and (ii) whether the topographic element is a ridge or a trough. Consequently, as the model results illustrate, the advection of the ambient potential vorticity field by the approaching monopole induces topographic beta-gyres of fundamentally different character for different values of y_0 and for different polarities of A. The outcome of a vortex–topography interaction is thus determined by the topography-induced deformation of the background vorticity field due to the β-effect. And this deformation is larger for initial positions more to the north or south and for higher ridges and deeper troughs.

Acknowledgements

The research described in this paper is financed by the TMR-MAST programme of the European Union (MAS3-CT96-5012, DG12-ASAL). The authors gratefully acknowledge this support. The comments of two anonymous reviewers led to substantial improvements in the text and the authors are pleased to thank them for their generosity.

References

Arakawa, A., 1966. Computational design for long-term numerical integration of the equations of fluid motion: two-dimensional incompressible flow. Part I. J. Comp. Phys. 1, 119–143.

Bograd, S.J., Rabinovich, A.B., LeBlond, P.H., Shore, J.A., 1997. Observations of seamount-attached eddies in the North Pacific. J. Geophys. Res. 102 (C6), 12,441–12,456.

Bower, A.S., Armi, L., Ambar, I., 1995. Direct evidence of meddy formation off the southwestern coast of Portugal. Deep-Sea Res. 42, 1621–1630.

Kamenkovich, V.M., Leonov, Y.P, Nechaev, D.A., Byrne, D.A., Gordon, A.L., 1996. On the influence of bottom topography on the Agulhas eddy. J. Phys. Ocean. 26, 892–912.

Korotaev, G.K., Fedotov, A.B., 1994. Dynamics of an isolated barotropic eddy on a beta-plane. J. Fluid Mech. 264, 277–301.

Llewellyn-Smith, S.G., 1997. The motion of a non-isolated vortex on the beta-plane. J. Fluid Mech. 346, 149–179.

Reznik, G.M., Dewar, W.K., 1994. An analytical theory of distributed axisymetric barotropic vortices on the β-plane. J. Fluid Mech. 269, 301–321.

Richardson, P.L., 1993a. Tracking ocean eddies. Amer. Sci. 81, 261–271.
Richardson, P.L., 1993b. A census of eddies observed in North Atlantic SOFAR float data. Prog. Oceanogr. 31, 1–50.
Sutyrin, G.G., Flierl, G.R., 1994. Intense vortex motion on the beta plane: development of the beta gyres. J. Atmos. Sci. 51, 773–790.
Van Geffen, J.H.G.M., Davies, P.A., 1999. Interaction of a monopolar vortex with a topographic ridge. Geophys. Astrophys. Fluid Dyn. 90, 1–41.
Van Geffen, J.H.G.M., Meleshko, V.V., Van Heijst, G.J.F., 1996. Motion of a two-dimensional monopolar vortex in a bounded rectangular domain. Phys. Fluids 8, 2393–2399.
Van Heijst, G.J.F., 1994. Topography effects on vortices in a rotating fluid. Meccanica 29, 431–451.